Pergamon

Int. J. Heat Mass Transfer. Vol. 38, No. 7, pp. 1261–1269, 1995
Copyright © 1995 Elsevier Science Ltd
Printed in Great Britain. All rights reserved
0017–9310/95 $9.50 + 0.00

0017–9310(94)00241–X

Convective heat and mass transfer along an inclined heated plate with film evaporation

WEI-MON YAN

Department of Mechanical Engineering, Hua Fan College of Humanities and Technology, Shih Ting, Taipei, Taiwan 22305, Republic of China

and

CHYI-YEOU SOONG

Department of Aeronautic Engineering, Chung Cheng Institute of Technology, Taoyuan, Taiwan 33509, Republic of China

(*Received* 4 *January* 1994 *and in final form* 19 *July* 1994)

Abstract—The purpose of this work is to investigate the heat and mass transfer characteristics along an inclined heated plate over which the water at room temperature flows downward as a film. To model the detailed transport processes special attention is drawn to the phase equilibrium and gas–liquid interface matching conditions. An implicit finite difference method is employed to solve the coupled governing equations for liquid film and gas flow together with the interfacial matching conditions. Evaporation of water vapor into the gas stream is examined for various conditions. The results clearly show the importance of the latent heat transport connected with film vaporization at the gas–liquid interface. In addition, it is found that an increase in inclined angle ϕ, inlet liquid film thickness δ or free stream velocity u_∞ causes reductions in the wall and interfacial temperatures.

1. INTRODUCTION

Gas–liquid flow systems with coupled heat and mass transfer are widely encountered in practice. Liquid film evaporator, turbine blade cooling, cooling of microelectronic equipments, protection of system components from high-temperature gas streams in supersonic aircraft and combustion chambers, and the simultaneous diffusion of metabolic heat and perspiration in the control of our body temperature are just some examples. Because of such widespread applications, evaporating liquid film flow and related problems have received considerable attention.

Mass transfer measurements have been reported for internal flows with moving liquid vapor interface [1, 2]. They showed that the effect of the reverse velocity at the gas–liquid interface reduces the mass transfer rate. In these studies, heat transfer was not considered. In a theoretical study, Howard and Lightfoot [3] extended the surface stretch model to the case of gas absorption into a laminar cocurrent film. No resistance to mass transfer was assumed to exist in the gas phase. By using an orthogonal expansion technique, Nunge and Gill [4] solved the energy equation for a countercurrent fully developed flow between two parallel plates.

Heat and mass transfer over a vertical falling film have been examined numerically and experimentally by Chandra and Savery [5, 6]. In their theoretical work the measured temperature and concentration distributions along the gas–liquid interface were used to specify the inhomogeneous boundary conditions required for solving the energy and species diffusion equations of air–vapor flow. In addition, a zero gas–liquid interfacial velocity was assumed. Evaporation of water film into a gas stream along a flat plate was investigated by Schroppel and Thiele [7], Chow and Chung [8, 9]. Their analyses [7–9] were restricted to the processes with negligible effects of liquid film; therefore, only the heat and mass transfer in the air stream were considered. Recently, the evaporation rates of water were measured by Haji and Chow [10] and the results agreed well with the predictions [8, 9] if the heat loss from the water pan was accounted for.

In practical situations, the liquid film along the wetted wall has a finite thickness, and thus the effects of the momentum and energy transports in the liquid film on the heat and mass transfer in the gas flow should be considered in the analysis. In this connection, the effect of a liquid film on the forced convection heat and mass transfer in gas stream has been treated in some studies [11–13]. In these studies the Nusselt-type approximation was adopted to simplify the treatment of the transports in the liquid film. Instead of employing such an approximation, a detailed analysis, including the transport processes in the gas flow and liquid film, was carried out by Yan [14] to investigate the effect of a finite liquid film on laminar convective heat and mass transfer in a vertical channel. Evaporating heat and mass transfer over a falling film along

NOMENCLATURE

A^+ damping-length constant
C_1, C_2, C_μ constants appearing in turbulent k–ε equations
c_p specific heat [J (kg·K)$^{-1}$]
c_{pa} specific heat for air [J (kg·K)$^{-1}$]
c_{pv} specific heat for water vapor [J (kg·K)$^{-1}$]
D mass diffusivity [m^2 s^{-1}]
f_2, f_μ functions appearing in turbulent k–ε equations
g gravitational acceleration [m s^{-2}]
h_{fg} latent heat of vaporization [J kg^{-1}]
h_M mass transfer coefficient
k turbulent kinetic energy [m^2 s^{-2}]
ℓ reference length, $\ell = 1.5$ m
$\dot{m}_I''$ interfacial mass flux [kg (s·m^2)$^{-1}$]
M_a molar mass of air [kg (K·mol)$^{-1}$]
M_v molar mass of vapor [kg (K·mol)$^{-1}$]
Nu_ℓ interfacial Nusselt number for latent heat transport, equation (22)
Nu_s interfacial Nusselt number for sensible heat transport, equation (21)
Nu_x overall Nusselt number $= Nu_s + Nu_\ell$, equation (20)
p_I partial pressure of water vapor at the gas–liquid interface [kPa]
Pr_ℓ Prandtl number of the liquid film
p_∞ mixture pressure at the free stream [kPa]
q_I'' total interfacial energy flux in gas side, equation (18) [W m^{-2}]
$q_{\ell I}''$ interfacial latent heat flux in gas side (or net enthalpy flux), $\dot{m}_I'' \cdot h_{fg}$ [W m^{-2}]
q_{SI}'' interfacial sensible heat flux in gas side [W m^{-2}]
q_w'' wall heat flux [W m^{-2}]
r dimensionless wall coordinate, $y \cdot u_*/\nu$
R_t turbulent Reynolds number $k^2/(\nu\varepsilon)$
Sh interfacial Sherwood number
T temperature [K, °C]
$T_{\ell i}$ inlet liquid film temperature [K, °C]
T_I gas–liquid interface temperature [K, °C]
T_∞ free-stream temperature [K, °C]
u axial velocity [m s^{-1}]
u_∞ free-stream velocity [m s^{-1}]
u_* shear stress velocity $(\tau_w/\rho)^{1/2}$
v transverse velocity [m s^{-1}]
w mass fraction of water vapor
w_I mass fraction of vapor at gas–liquid interface
x coordinate in the flow direction [m]
X dimensionless coordinate in the flow direction x/ℓ
y coordinate in the transverse direction [m]
y^+ dimensionless wall coordinate $(y-\delta_x)\cdot u_*/\nu$.

Greek symbols

δ inlet liquid film thickness [m]
δ_x local liquid film thickness [m]
ε the rate of dissipation of turbulent kinetic energy [m^2 s^{-3}]
λ molecular thermal conductivity [W (m^{-1}·°C)$^{-1}$]
λ_t turbulent eddy conductivity [W (m^{-1}·°C)$^{-1}$]
τ_I shear force at the gas–liquid interface [kPa]
τ_w wall shear stress [kPa]
μ molecular dynamic viscosity [N·s m^{-2}]
μ_t turbulent eddy viscosity [N·s m^{-2}]
ρ density [kg m^{-3}]
ϕ inclined angle of the heated plate
σ_k turbulent Prandtl number for k
σ_ε turbulent Prandtl number for ε.

Subscripts

a of air
I condition at the gas–liquid interface
g of mixture (air + water vapor)
ℓ of liquid
t turbulent
v of vapor
w condition at wall
∞ condition at the inlet or free stream.

a vertical heated plate were experimentally studied by Lin [15]. Recently, Yan and Soong [16] investigated liquid film cooling in a turbulent gas stream. In their study, it is disclosed that the introduction of a thin continuous liquid film onto a given surface can effectively protect the wetted surface from thermal damage by the proximate hot gas stream. Although the flow over a vaporizing liquid film along an inclined heated plate is relatively important in practical applications, it has received relatively little attention. The objective of this work is to investigate the influences of various parameters such as the inclined angle, wall heating flux, inlet liquid film thickness and free stream velocity on the evaporation processes along the gas–liquid interface.

2. ANALYSIS

The problem under consideration, as shown schematically in Fig. 1, concerns a large plate with inclined

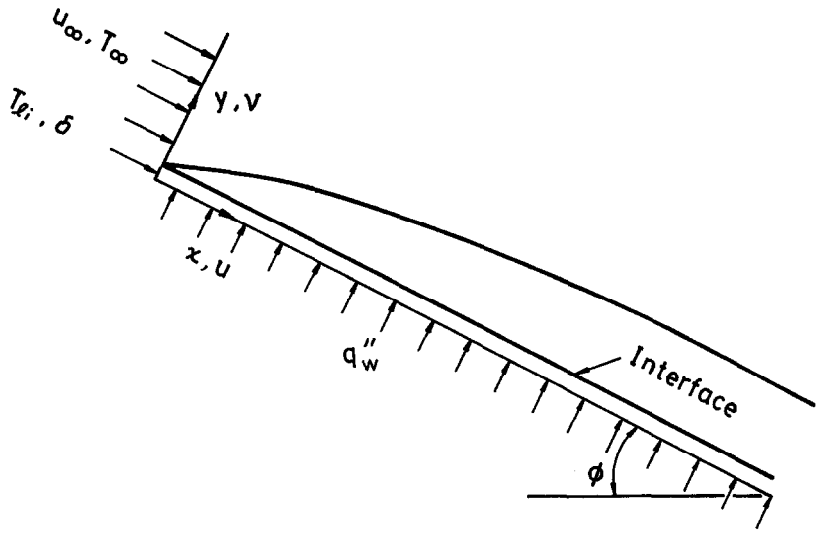

Fig. 1. Schematic diagram of the physical system.

angle ϕ. A uniform heat flux q''_w is imposed on the inclined plate. The plate is wetted by a water film fed at a room temperature $T_{\ell i}$ and an inlet film thickness δ. The water film falls down the inclined plate due to the action of gravity and is exposed to a downward gas flow at free-stream velocity u_∞ and ambient temperature T_∞. Heat is transferred from the heated plate to the liquid film and across which to the gas stream. Meanwhile, simultaneous mass transfer from the water film to the gas stream occurs as the the liquid film vaporizes.

2.1. *Basic equations for liquid film*

As shown in Dukler's work [17], the surface waves on a falling liquid film at $Re_\ell > 16$ normally appear except in the region near the start of the flow. The waves are of three-dimensional and unsteady characters. Due to the complexity of the wave motion, an assumption of time-wise steady film thickness used in numerous investigations [18–20] is adopted in the present study. This steady film thickness can be interpreted as the temporal average of the large amplitude waves on the surface of the actual film [19]. Additionally, to facilitate the analysis, the inertia terms in the liquid–film momentum equation are neglected as compared with the diffusion term [11–13]. Therefore, the two-dimensional boundary layer flow in the turbulent liquid film is governed by the axial-momentum and energy equations:

$$\partial[(\mu_\ell + \mu_{\ell t})\partial u_\ell/\partial y]/\partial y + \rho_\ell g \cdot \sin\phi = 0 \quad (1)$$

$$\rho_\ell c_{p\ell} u_\ell \partial T_\ell/\partial x = \partial[(\lambda_\ell + \lambda_{\ell t})\partial T_\ell/\partial y]/\partial y \quad (2)$$

where $\mu_{\ell t}$ and $\lambda_{\ell t}$ are the turbulent viscosity and turbulent conductivity, and will be modeled in Section 3.

2.2. *Basic equations for gas stream*

Steady turbulent forced convection heat and mass transfer in the gas flow can be explored, with the usual boundary layer approximations, by the following gas-side conservation equations of mass, axial-momentum, energy and concentration:

$$\partial(\rho_g u_g)/\partial x + \partial(\rho_g v_g)/\partial y = 0 \quad (3)$$

$$\rho_g u_g \partial u_g/\partial x + \rho_g v_g \partial u_g/\partial y = \partial[(\mu_g + \mu_{gt})\partial u_g/\partial y]/\partial y \quad (4)$$

$$\rho_g c_{pg} u_g \partial T_g/\partial x + \rho_g c_{pg} v_g \partial T_g/\partial y = \partial[(\lambda_g + \lambda_{gt})\partial T_g/\partial y]/\partial y \quad (5)$$

$$\rho_g u_g \partial w/\partial x + \rho_g v_g \partial w/\partial y = \partial[\rho_g (D + D_t)\partial w/\partial y]/\partial y. \quad (6)$$

Where the μ_{gt}, λ_{gt} and D_t denote the turbulent viscosity, conductivity and mass diffusivity of the binary gas mixture, respectively. In Section 3, these turbulent flow properties will be modeled properly.

2.3. *Boundary and interfacial matching conditions*

The boundary conditions for this problem are:

$$x = 0: \quad u_g = u_\infty, T_g = T_\infty, T_\ell = T_{\ell i}, w = w_\infty \quad (7)$$

$$y = 0: \quad u_\ell = 0, -(\lambda_\ell + \lambda_{\ell t})\,\partial T_\ell/\partial y = q''_w \quad (8)$$

$$y = \delta_x: \quad u_g = u_\ell, T_g = T_\ell, w = w_I(x) \quad (9)$$

$$y \to \infty: \quad u_g = u_\infty, T_g = T_\infty, w = w_\infty. \quad (10)$$

At the interface ($y = \delta_x$), the gas- and liquid-side solutions must be matched by satisfying the following conditions:

(1) Continuity of velocity

$$u_I(x) = u_{g,I} = u_{\ell,I}. \quad (11)$$

(2) Continuity of temperature

$$T_I(x) = T_{g,I} = T_{\ell,I}. \quad (12)$$

(3) Continuity of shear stress

$$\tau_I(x) = [(\mu+\mu_t)\partial u/\partial y)]_{g,I} = [(\mu+\mu_t)\partial u/\partial y]_{\ell,I}. \quad (13)$$

(4) Transverse velocity of the air–vapor mixture is deduced by assuming the interface is semipermeable [21], that is, the solubility of air in the liquid film is negligibly small and y-component of air velocity is zero at the interface:

$$v_I = -(D+D_t)/(1-w_I)\cdot\partial w/\partial y. \quad (14)$$

(5) By assuming the interface to be in thermodynamic equilibrium and the air–vapor mixture an ideal gas mixture, the mass fraction of the vapor can be evaluated by [21]

$$w_I = M_v p_I/[M_a(p-p_I)+M_v p_I] \quad (15)$$

where p_I is the partial pressure of the vapor at the gas–liquid interface. M_v and M_a denote the molar mass of vapor and air, respectively.

(6) Vaporizing flux of vapor into the gas flow is

$$\dot{m}_I'' = -\rho(D+D_t)/(1-w_I)\cdot\partial w/\partial y. \quad (16)$$

(7) Energy balance at the gas–liquid interface

$$[-(\lambda+\lambda_t)\partial T/\partial y]_{\ell,I} = [-(\lambda+\lambda_t)\partial T/\partial y]_{g,I}+\dot{m}_I''\cdot h_{fg}. \quad (17)$$

The above equation states that at the interface the energy can be transported into the gas stream in two modes. One is the sensible heat transfer via the gas temperature gradient, q_{SI}''. The other is through the latent heat transfer via the liquid film vaporization, $q_{\ell I}''$. Therefore, the total interfacial heat transfer from the liquid to the gas stream, q_I'', can be expressed as

$$q_I'' = q_{SI}''+q_{\ell I}'' = -[(\lambda+\lambda_t)\partial T/\partial y]_{g,I}+\dot{m}_I''\cdot h_{fg}. \quad (18)$$

The local Nusselt number at the interface, defined as

$$Nu_x = h\cdot x/\lambda_g = q_I''\cdot x/[\lambda_g(T_I-T_\infty)] \quad (19)$$

can be written as

$$Nu_x = Nu_s+Nu_\ell \quad (20)$$

where Nu_s and Nu_ℓ are, respectively, the local Nusselt numbers for sensible and latent heat transfer, and are defined as

$$Nu_s = x\cdot q_{SI}''/[\lambda_g(T_I-T_\infty)] \quad (21)$$

and

$$Nu_\ell = x(\dot{m}_I''\cdot h_{fg})/[\lambda_g(T_I-T_\infty)]. \quad (22)$$

Similarly, the Sherwood number is defined as

$$Sh = h_M\cdot x/D = x\cdot\dot{m}_I''(1-w_I)/[\rho_g D(w_I-w_\infty)]. \quad (23)$$

In the above formulation the variations of the thermophysical properties with temperature and mixture composition are considered. They are calculated from the pure component data by means of mixing rules [22, 23] applicable to any multicomponent mixtures. The pure component data [24] are approximated by polynomials in terms of temperature. The complete details on the evaluation of these properties are available in the work of Fuji *et al.* [24].

3. TURBULENCE MODELING

3.1. *Liquid film*

To compute the velocity profile of the liquid film, a model for turbulent eddy viscosity $\mu_{\ell t}$ is required. In this work a modified van Driest model proposed by Yih and Liu [20] was used herein. Therefore, for $y/\delta \leqslant 0.6$, the eddy viscosity is evaluated by

$$\frac{\mu_{\ell t}}{\mu_\ell} = -0.5+0.5\{1+0.64r^2(\tau/\tau_w)\cdot[1-\exp(-r(\tau/\tau_w)^{1/2}/25.1)]^2 f^2\}^{1/2} \quad (24)$$

where $f = \exp[-1.66(1-\tau/\tau_w)]$ is a damping factor. For $0.6 \leqslant y/\delta_x \leqslant 1$, the turbulent eddy viscosity for the liquid film is taken as constant and equals to the value at $y/\delta_x = 0.6$ obtained from equation (24). Note that equation (24) differs from the model used by Limberg [25] and Seban and Faghri [19]. In the former the shear stress and damping factor terms are modified to include the effect of interfacial shear.

In the aforementioned turbulence model, the effects of interfacial shear and wave have been taken into account [20]. In some previous studies [18, 19], similar models were successfully applied to the analysis of heat transfer across a turbulent falling film with an assumption of time-wise steady film thickness. This lends support to the employment of the time-wise steady film thickness assumption to the analysis of this class of liquid film flow.

3.2. *Gas flow*

For simulation of turbulence in the gas flow, a modified low Reynolds number k–ε model developed by Myong *et al.* [26, 27] is adopted, in which the equations for turbulent kinetic energy and its dissipation rate are:

$$\rho u\,\partial k/\partial x+\rho v\,\partial k/\partial y = \partial[(\mu+\mu_t/\sigma_k)\,\partial k/\partial y]/\partial y+\mu_t(\partial u/\partial y)^2-\rho\varepsilon \quad (25)$$

$$\rho u\,\partial\varepsilon/\partial x+\rho v\,\partial\varepsilon/\partial y = \partial[(\mu+\mu_t/\sigma_\varepsilon)\,\partial\varepsilon/\partial y]/\partial y+C_1(\varepsilon/k)\mu_t(\partial u/\partial y)^2-\rho C_2 f_2\varepsilon^2/k \quad (26)$$

where

$$\mu_t = \rho C_\mu f_\mu k^2/\varepsilon \quad (27)$$

$$f_2 = \{1-2/9\cdot\exp[-(R_t/6)^2]\}[1-\exp(-y^+/5)]^2 \quad (28)$$

$$f_\mu = (1+3.45/\sqrt{R_t})\cdot[1-\exp(-r/70)] \quad (29)$$

$$R_t = k^2/(v\varepsilon),\quad y^+ = (y-\delta_x)u_*/v,\quad u_* = (\tau_w/\rho)^{1/2}. \quad (30)$$

The other empirical constants take the following values [26, 27]:

Table 1. Comparisons of local Sherwood number Sh for various grid arrangements for $\phi = 45°$, $q''_w = 3 \times 10^4$ W m^{-2}, $\delta = 7.5 \times 10^{-4}$ m and $u_\infty = 40$ m s^{-1}

X	$I \times J \times K$†				
	$201 \times 241 \times 81$	$101 \times 241 \times 81$	$101 \times 121 \times 41$	$101 \times 61 \times 21$	$51 \times 61 \times 21$
0.0641	427.55	425.64	428.70	379.39	415.62
0.1242	745.43	746.22	749.83	672.73	730.34
0.2005	1118.14	1120.17	1123.67	1019.72	1094.32
0.4086	2065.95	2071.15	2073.56	1915.03	2022.53
0.6053	2932.85	2932.37	2935.59	2734.96	2916.55
0.8106	3814.82	3811.91	3820.46	3587.01	3788.27
1.0	4615.47	4614.82	4634.60	4374.89	4656.14

†I = Total grid points placed in the longitudinal direction, J = total grid points placed in the transverse direction in the gas-side, K = total grid points placed in the transverse direction in the liquid-side.

$$\sigma_k = 1.4, \quad \sigma_\varepsilon = 1.3, \quad C_1 = 1.4,$$
$$C_2 = 1.8, \quad C_\mu = 0.09. \tag{31}$$

4. SOLUTION METHOD

In view of the complicated couplings between the transport processes in the gas stream and the liquid film, the problem is solved numerically using a fully implicit numerical scheme. The axial convective term is approximated by upwind difference, and the transverse convection and diffusion terms by central difference form. At the gas–liquid interface, the matching conditions for the continuities of shear stress and heat flux were recast in backward difference for $(\partial\psi/\partial y)_l$ and forward difference for $(\partial\psi/\partial y)_g$ with ψ denoting u or T. Therefore, the governing equations in the gas flow and liquid film can be solved simultaneously by a line-by-line method [28]. It is important to note that the system of finite difference equations forms a tridiagonal set which can be efficiently solved by the Thomas algorithm [28].

To obtain enhanced accuracy in numerical computations, grids are nonuniformly distributed in both axial and transverse directions to account for the uneven variations of u, T and w. The grid are transversely clustered near the gas–liquid interface, and the grid density is also higher in the region near the inlet. The transverse distribution of grid nodes is arranged by locating the first five nodes in the gas-side within the viscous sublayer adjacent to the gas–liquid interface and expanding the rest of the grid points to the free stream using a factor of 1.04. To produce grid-independent results, numerical experiments for several grid arrangements are performed and a comparison of the local Sherwood number Sh for a typical case is given in Table 1. It is noted that the differences in the local Sherwood numbers from computations using either $201 \times 241 \times 81$ or $101 \times 121 \times 41$ grids are always less than 1%. Accordingly, the computations involving a $101 \times 121 \times 41$ grid are considered to be sufficiently accurate to describe the heat and mass transfer in the present wetted wall system. All the results presented in Section 5 were computed using the latter grid. To further check the numerical scheme, the results for limiting cases of laminar and turbulent convection heat and mass transfer along a wetted flat plate were first obtained. The present predictions agree well with those of refs. [7, 8].

5. RESULTS AND DISCUSSION

The system parameters, including the inclined angle ϕ, wall heating flux q''_w, free-stream velocity u_∞ and temperature T_∞, inlet film thickness δ, and inlet film temperature T_{fi}, appear in the preceding analysis. Naturally, a complete parametric study is unrealistic for such a complex system. To reduce the computational efforts, the parameters were varied systematically in order to examine the key trends of the solution behaviors. The parameters ranges considered in this work are: $0° \leqslant \phi \leqslant 90°$, $1 \times 10^4 \leqslant q''_w \leqslant 5 \times 10^4$ W m^{-2}, $5 \times 10^{-4} \leqslant \delta \leqslant 1 \times 10^{-3}$ m, $20 \leqslant u_\infty \leqslant 60$ m s^{-1} and $T_{fi} = T_\infty = 20°$C. Since the main concerns are the water film evaporation, the attention is then focused on the influences of ϕ, q''_w, δ and u_∞ on the transport phenomena in vaporizing water film.

To illustrate the effects of various parameters on the wall and interfacial temperatures Fig. 2 presents the axial distributions of T_w and T_I. An inspection on these plots reveals that T_w and T_I increase monotonically with the axial location X. This is attributed to the continuous heating from the heated plate. Note that $X = x/\ell$ is a nondimensional coordinate in the x-direction, where the reference length ℓ is selected as 1.5 m. As expected, T_w and T_I are higher for systems with a smaller inclined angle ϕ and free-stream velocity u_∞. These are shown in Fig. 2(a) and (d). In Fig. 2(b), higher T_w and T_I are noted for a higher q''_w. This is due to a higher heating flux from the heated plate to the water film. Figure 2(c) gives the effect of inlet film thickness δ on the distributions of T_w and T_I. Lower T_w and T_I are experienced by a system of a larger δ, for which a larger liquid mass flow rate is resulted.

The effects of inclined angle and wall heat flux on the interfacial mass fraction of water vapor along the gas–liquid interface are depicted in Fig. 3. As shown in Fig. 2(a) and (b), a higher interfacial temperature

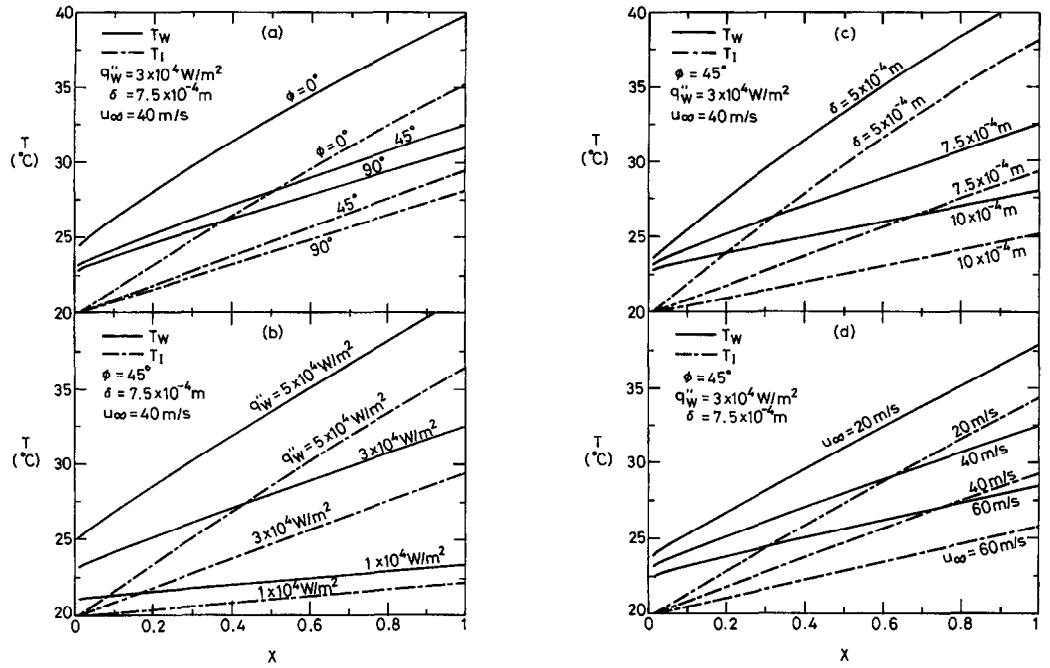

Fig. 2. Axial distributions of wall temperature and interfacial temperature.

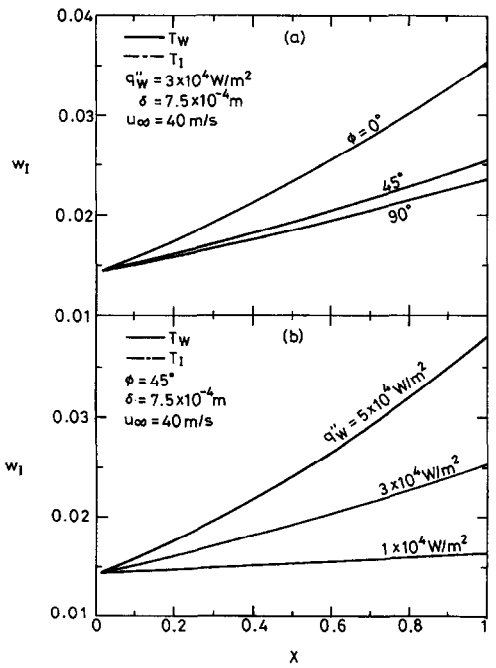

Fig. 3. Axial distributions of interfacial mass fraction of water vapor.

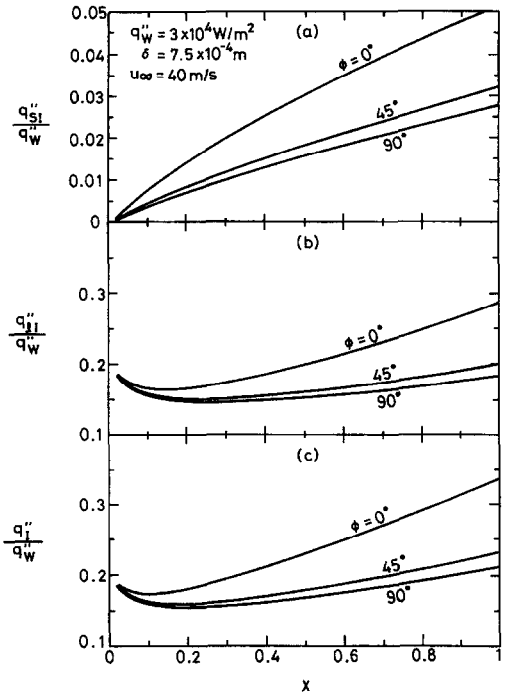

Fig. 4. Distributions of local dimensionless heat transfer rates in the gas-side along the inclined plate: (a) interfacial sensible heat flux, (b) interfacial latent heat flux, (c) total heat flux.

T_I can be resulted for a smaller inclined angle ϕ or a higher wall heating flux q''_w. Therefore, the corresponding mass fraction of the water vapor along the gas–liquid interface is larger for a smaller ϕ or a higher q''_w.

It is interesting to investigate the relative importance of the sensible and latent heat exchanges along the gas–liquid interface. Figure 4 presents the axial distributions of heat transfer rates along the gas–liquid interface. In Fig. 4(a), the sensible heat flux q''_{SI}/q''_w increases in the flow direction but decreases with the inclined angle ϕ. For the latent heat exchange, q''_{rI}/q''_w decreases first with X. After reaching

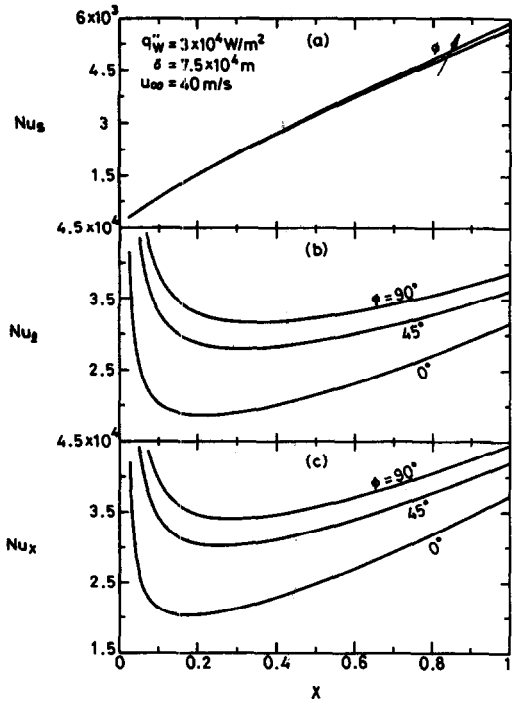

Fig. 5. Local Nusselt number distributions along the inclined plate: (a) sensible heat Nusselt number, (b) latent heat Nusselt number, (c) interfacial Nusselt number.

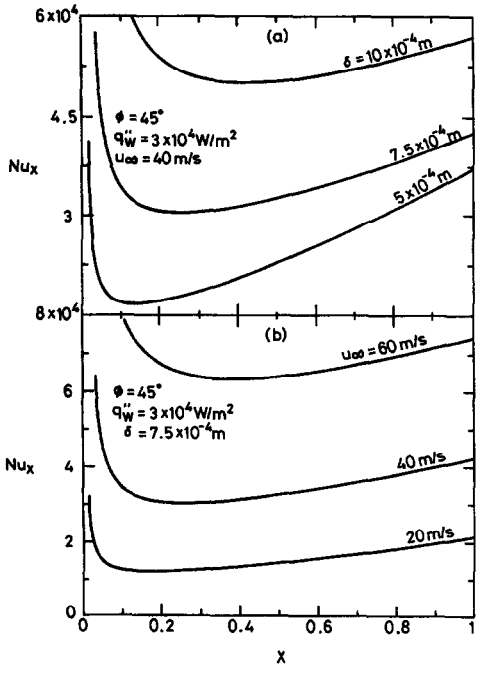

Fig. 6. Effects of inlet film thickness δ and free-stream velocity u_∞ on the interfacial Nusselt number.

a local minimum, the latent heat flux increases monotonically in the flow direction. Even at $\phi = 0°$, q''_{sl}/q''_w is always below 6%, but $q''_{\ell l}/q''_w$ can be above 25%. For a fixed ϕ, $q''_{\ell l}$ is about six times larger than q''_{sl}. The results in Fig. 4(c) indicate that, at a large ϕ (= 90°), most of the heat input to the system goes to heat up the liquid film and less than 22% of the heat input transfers across the film to cause film vaporization and air temperature rise.

To improve understanding of the interfacial heat transfer, the variations of the local Nusselt numbers for the sensible and latent heat transfer at the interface are shown in Fig. 5 for various inclined angles ϕ. According to the results in Fig. 5(a), Nu_s increases slightly with ϕ. A larger Nu_ℓ is noted for a system with a larger ϕ. It is noted that the actual sensible and latent heat transfer rates, as shown in Fig. 4, reduce with increasing ϕ. These results clearly indicate that the magnitudes of the Nusselt numbers do not reflect the actual heat transfer rates. The anomaly in the Nusselt numbers defined in equations (21) and (22) results from the larger effect of the inclined angle ϕ on the interface temperature T_I than on the q''_{sl} and $q''_{\ell l}$, as is evident from Figs. 2 and 4. Comparing the ordinate scales of Fig. 5(a) and (b) indicates that the magnitude of Nu_ℓ is much larger than that of Nu_s. This demonstrates that the interfacial heat transfer resulting from latent heat exchange is much more effective. Shown in Fig. 5(c) is the effect of inclined angle ϕ on the total interfacial Nusselt number Nu_x $(= Nu_s + Nu_\ell)$.

To further enhance our understanding on the influences of the inlet film thickness δ and free stream velocity u_∞ on the interfacial Nusselt number Nu_x, Fig. 6 gives these two parameters on the local Nusselt number distributions. It is clearly observed in Fig. 6(a) that a larger Nu_x can be resulted for a larger inlet film thickness δ. This confirms the general conception that, for a falling film, the heat transfer is enhanced for systems with a larger inlet film thickness or inlet liquid mass flow rate. Results are also found in Fig. 6(b) for the effect of u_∞ on Nu_x distributions. It can be seen that Nu_x increases with u_∞. This result is similar to the usual single phase forced convection heat transfer along a plate.

To illustrate the mass transfer characteristics, the distributions of the interfacial mass evaporation rate and Sherwood number are presented in Fig. 7 for various inclined angles ϕ. Similar to the results of $q''_{\ell l}/q''_w$ given in Fig. 4(b), a reduction in the inclined angle ϕ causes a greater film evaporation. This outcome apparently is due to the higher interfacial temperature at a smaller ϕ, as shown in Fig. 2(a). The change in the inclined angle ϕ has an insignificant influence on the Sherwood number, as is evident from Fig. 7(b).

The effects of the imposed wall heat flux q''_w and free-stream velocity u_∞ on the mass transfer coefficient are of interest. In Fig. 8(a) the Sherwood number Sh monotonically increases in the flow direction and an increase in q''_w leads to an increase in Sh. In Fig. 8(b), a higher u_∞ results in a larger Sh, like the u_∞ effect in Fig. 6(b).

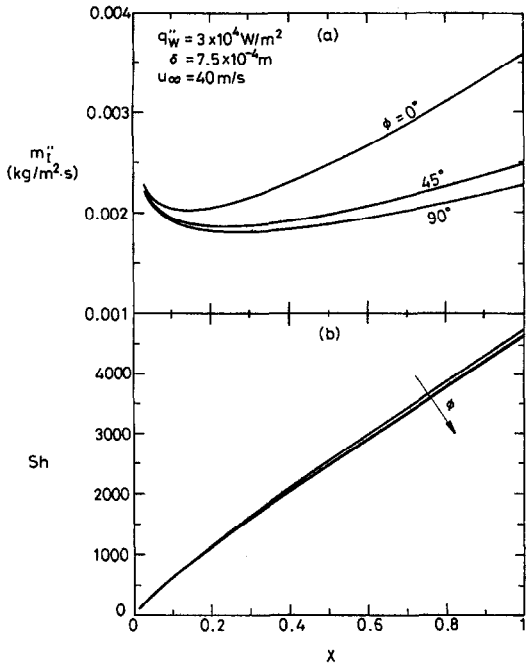

Fig. 7. Effects of inclined angle ϕ on the local interfacial mass evaporation rate and Sherwood number distributions.

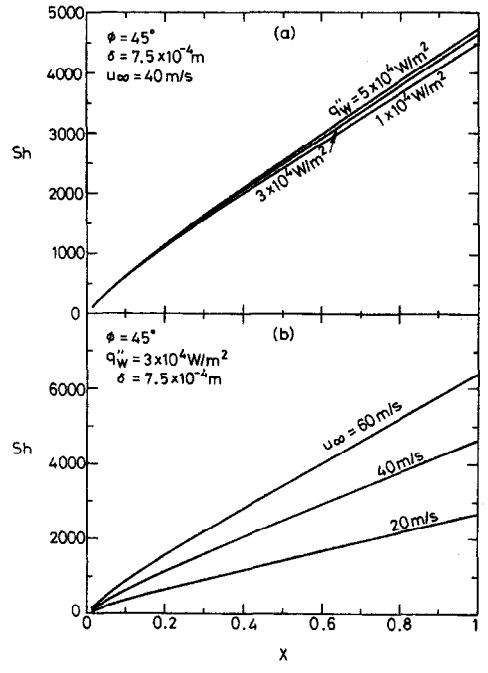

Fig. 8. Effects of wall heat flux q''_w and free-stream velocity u_∞ on the variations of Sherwood number *Sh*.

6. CONCLUSIONS

The evaporation of water vapor along the inclined heated plate has been investigated numerically. The influences of the inclined angle ϕ, wall heating flux q''_w, inlet film thickness δ and free-stream velocity u_∞ on the momentum, heat and mass transfer in the system are the major concerns in the study. From the present results, the following conclusions can be drawn:

(1) Heat transfer between the liquid film and turbulent gas stream is dominated by the transport of latent heat connected with film evaporation. The magnitude of the evaporative latent heat flux may be six times greater than that of the sensible heat flux.

(2) A reduction in the inclined angle ϕ causes an increase in the interfacial temperature T_I, which in turn leads to a larger latent heat exchange. This is brought about by the larger latent heat transport associated with a greater film vaporization for a higher T_I.

(3) The local heat transfer performance characterized by Nu_x increases with the plate inclination, ϕ, film thickness, δ, and gas-stream velocity, u_∞.

(4) Mass transfer rate can be enhanced in the systems with a higher wall heat flux or gas-stream velocity.

Acknowledgement—The financial support of this research by the National Science Council, Republic of China, through the contract NSC 81-0401-E014-01 is greatly appreciated.

REFERENCES

1. C. H. Byers and C. J. King, Gas–liquid mass transfer with a tangentially moving interface: Part 1 and 2, *A.I.Ch.E. Jl* **13**, 628–644 (1967).
2. M. W. Clark and C. J. King, Evaporation rates of volatile liquids in a laminar flow system: Part 1 and 2, *A.I.Ch.E. Jl* **16**, 64–75 (1970).
3. D. W. Howard and E. N. Lightfood, Mass transfer to falling film: Part 1, *A.I.Ch.E. Jl* **14**, 458–467 (1968).
4. R. J. Nunge and W. N. Gill, Analysis of heat or mass transfer in some countercurrent flows, *Int. J. Heat Mass Transfer* **8**, 873–886 (1965).
5. V. Chandra and C. W. Savery, Forced convection heat and mass transfer from a falling film to a laminar external boundary layer, *Int. J. Heat Mass Transfer* **17**, 1549–1557 (1974).
6. V. Chandra, Mass, momentum and heat transfer from a falling film to a countercurrent air stream, Ph.D. Thesis, Department of Mechanical Engineering, Drexel University (1975).
7. J. Schroppel and F. Thiele, On the calculation of momentum, heat and mass transfer in laminar and turbulent boundary layer flow along a vaporizing liquid film, *Numer. Heat Transfer* **6**, 475–496 (1983).
8. L. C. Chow and J. N. Chung, Evaporation of water into a laminar stream of air and superheated steam, *Int. J. Heat Mass Transfer* **26**, 373–380 (1983).
9. L. C. Chow and J. N. Chung, Water evaporation into a turbulent stream of air, humid air or superheated steam, 21st ASME/AIChE National Heat Transfer Conference, Seattle, WA, ASME Paper No. 83-HT-2 (1983).
10. M. Haji and L. C. Chow, Experimental measurement of water evaporation rates into air and superheated steam, *J. Heat Transfer* **110**, 237–242 (1988).
11. T. R. Shembharkar and B. R. Pai, Prediction of film cooling with a liquid coolant, *Int. J. Heat Mass Transfer* **29**, 899–908 (1986).
12. W. W. Baumann and F. Thiele, Heat and mass transfer in two-component film evaporation in a vertical tube, *Proceedings of the 8th International Heat Transfer Conference*, Vol. 4, pp. 1843–1848 (1986).
13. W. W. Baumann and F. Thiele, Heat and mass transfer

in evaporating two-component liquid film flow, *Int. J. Heat Mass Transfer* **33,** 267–273 (1990).
14. W. M. Yan, Effects of film evaporation on laminar mixed convection heat and mass transfer in a vertical channel, *Int. J. Heat Mass Transfer* **35,** 3419–3429 (1992).
15. T. F. Lin, Heat transfer enhancement through latent heat transport in mixed convection, NSC Report, No. 80-0401-E009-14 (1992).
16. W. M. Yan and C. Y. Soong, Numerical study of liquid film cooling in a turbulent gas stream, *Int. J. Heat Mass Transfer* **36,** 3877–3885 (1993).
17. A. E. Dukler, Characterization, effects and modeling of the wavy gas–liquid interface, *Prog. Heat Mass Transfer* **6,** 207–234 (1972).
18. G. L. Hubbard, A. F. Mills and D. K. Chung, Heat transfer across a turbulent falling film with cocurrent vapor flow, *J. Heat Transfer* **98,** 319–320 (1976).
19. R. A. Seban and A. Faghri, Evaporation and heating with turbulent falling liquid films, *J. Heat Transfer* **98,** 315–318 (1976).
20. S. M. Yih and J. L. Liu, Falling liquid film with or without interfacial shear, *A.I.Ch.E. Jl* **29,** 903–909 (1983).
21. E. R. G. Eckert and R. M. Drake, Jr, *Analysis of Heat and Mass Transfer*. McGraw-Hill, New York (1972).
22. R. C. Reid, J. M. Prausnitz and T. K. Sherwood, *The Properties of Gases and Liquids*. McGraw-Hill, New York (1981).
23. R. B. Bird, W. E. Steward and E. N. Lightfood, *Transport Phenomena*. John Wiley, New York (1960).
24. T. Fujii, Y. Kato and K. Mihara, Expressions of transport and thermodynamic properties of air, steam and water, Sei San Ka Gaku Ken Kyu Jo, Report No. 66, Kyu Shu Dai Gaku, Kyu Shu (1977).
25. H. Limberg, Warmeubergang an turbulente und laminare rieselfilme, *Int. J. Heat Mass Transfer* **16,** 1691–1698 (1973).
26. H. K. Myong, N. Kasagi and M. Hira, Numerical prediction of turbulent pipe flow heat transfer for various Prandtl number fluids with the improved k–ε turbulence model, *JSME Int. J.* **32,** 613–622 (1989).
27. H. K. Myong and N. Kasagi, A new approach to the improvement of k–ε turbulence model for wall bounded shear flow, *JSME Int. J.* **33,** 63–72 (1990).
28. S. V. Patankar, *Numerical Heat Transfer and Fluid Flow*. Hemisphere/McGraw-Hill, New York (1980).